STATISTICAL BONE SHAPE ANALYSIS FOR IMAGE FREE SURGERY

Mauricio REYES AGUIRRE*, Marius George LINGURARU,**
Miguel Ángel GONZÁLEZ BALLESTER*

*Institute for Surgical Technology and Biomechanics, MEM Research Center, University of Bern, Stauffacherstrasse 78, CH-3014 Bern, Switzerland
**Division of Engineering and Applied Sciences, Harvard University, 60 Oxford Street, Cambridge, MA 01238, USA

mauricio.reyes@memcenter.unibe.ch

Abstract: Statistical shape analysis techniques employed in the medical imaging community, such as Active Shape Models or Active Appearance Models, rely on Principal Component Analysis (PCA) to decompose shape variability into a reduced set of interpretable components. Our model uses point distribution models (PDM) for the representation of shapes. The point association is initialized using shape-based surface correspondence and optimized with the Minimum Description Length (MDL) criterion. The model fitting algorithm is formulated as a least square error minimization regularized by the Mahalanobis distance of the predicted model. We present quantitative and qualitative results obtained for the case of statistical shape analysis of bones, with applications to image free surgery.

Key words: shape variability, principal component analysis, morphological analysis, computer assisted surgery.

1. Introduction

The analysis of shape variability of anatomical structures is of key importance in a number of clinical disciplines, as abnormality in shape can be related to certain diseases. Examples in neurology include the study of brain asymmetry to verify its relation to schizophrenia [1], or the detection and quantification of atrophy as a correlate to multiple sclerosis [2].

Statistical shape analysis techniques enjoy a remarkable popularity within the medical image analysis community. Its flagship, the Active Shape Model (ASM), proposed by Cootes et al. [3], provides a method to study the structure of point data sets or meshes [4]. This technique was later extended to intensity information, and thus image data, as the Active Appearance Model (AAM) [5].

In Computer Assisted Orthopaedic Surgery (CAOS), the use of statistical shape models for shape recovery from points digitized using a tracked pointer provides the surgeon a tool to improve the accuracy of surgical procedures in a minimally invasive fashion. These clinical utensils relax the need of having dedicated systems to create the shape models, like computed tomography (CT) or magnetic resonance imaging (MRI), which are expensive and/or induce radiation to the patient. Additionally, a number of orthopaedic interventions, such as total hip arthroplasty (THA) and total knee arthroplasty (TKA), do not warrant a pre- or intra-operative scan. The alternative is to build a statistical deformable model and adapt it to the patient anatomy.

In CAOS, this type of approach was initially explored by Fleute and Lavallée [6] and then clinically evaluated by Stindel and colleagues [7]. Both approaches fit the deformable model surface to intra-operatively digitized point data via jointly optimizing deformation and pose. In [8], optimization of both deformation and pose are performed separately using an iterative closest point (ICP) method. In [9] shape information coded by digitized points from the Principal Component Analysis (PCA) model is iteratively removed by fixing certain locations. The extrapolated surface is then computed as the most probable surface in the shape space given the data. Unlike earlier methods, this approach

can also able include non-spatial data, such as patient height and weight.

Section 2 presents the methodology used to construct the statistical shape model. First, a brief discussion about how point correspondences are found before a multivariate statistical analysis is performed is given. Then, the key concepts of principal component analysis and its application to medical image data are presented. Section 3 presents results obtained on shape analysis of proximal and full femur CT data, then results of reconstructing femur shape given sparse surface information from dry cadaver femur data.

2. Methodology

Several geometrical models have been proposed to represent and study shape variability. Bookstein [10] uses landmarks to capture the important geometric features. The active shape model (ASM) of Cootes and Taylor [3] represents the geometry of an object as a dense collection of boundary points, which was extended to include intensity information [5]. Kelemen et al. [11] use a spherical harmonic (SPHARM) decomposition of the object geometry. Others have explored the possibility of constructing a Statistical Shape Model Using Non-rigid Deformation of a Template Mesh [12].

To build our model, we employed the representation of shapes using point distribution models (PDM). One key issue is to establish correspondences between homologous points, i.e. find which points correspond to the same anatomical location among shapes.

2.1 Finding Point Correspondences

In 2D, correspondence is often established using manually determined landmarks, but this is a time-consuming, error-prone and subjective process. In principle, the method extends to 3D, but in practice, due to very small sets of reliably identifiable landmarks, manual landmarking becomes impractical. Most automated or semi-automated approaches posed the correspondence problem as that of defining a parameterization for each of the objects in the training set, assuming correspondence between equivalently parameterized points.

Current semi- and fully automated methodologies can be classified into two branches: Pairwise and Groupwise methods. In Pairwise methods, an initial shape is selected as reference and the rest of input shapes are then matched to this reference shape. Alternatively, the reference shape can be generated from the first match of shapes. These approaches can then be seen as a registration problem. Several algorithms have been proposed to solve this problem in the volumetric image space (i.e. image data) or as a surface matching task. Which method should be used will depend on the nature of the input data (e.g., laser-scanning, CT data). In Groupwise methods all the shapes of the training dataset are matched simultaneously through optimization of a groupwise objective function.

We compared the methods introduced by Brechbühler et al. (SPHARM) [13], Kotcheff and Taylor (DetCov) [14], Davies et al. (MDL) [15], and a fourth method based on manually initialized subdivision surfaces similar to Wang et al. (MSS) [16]. We analyzed both the direct correspondence via manually selected landmarks as well as the properties of the model implied by the correspondences, in regard to compactness, generalization and specificity. In a previous comparative study of these popular methods [17], it was revealed that for modelling purposes the best among the correspondence methods was Minimum Description Length (MDL) [15]. Based on the study, for our model building, correspondence was initialized using MSS and then optimized based on the MDL criterion.

2.2 Principal Component Analysis

PCA is a projection model for multivariate factor analysis aiming to find a low-dimensional manifold in the space of the data, such that the distance between the data and their projection on the manifold is small [18]. PCA is the best, in the mean-square error sense, linear dimension reduction technique [19].

Given a set of training data $\{t_1,\ldots,t_n\}$ in a given orthonormal basis of $\Re^D$, PCA finds a new orthonormal basis $\{u_1,\ldots,u_d\}$ with its axes ordered. This new basis is rotated such that the first axis is oriented along the direction in which the data has its highest variance. The second axis is oriented along the direction of maximal variance in the data, orthogonal to the first axis. Similarly, subsequent axes are oriented so as to account for as much as possible of the variance in the data, subject to the constraint that they must be orthogonal to the preceding axes. Consequently, these axes have associated decreasing indices λ_d, d=1,…,D, corresponding to the variance of the data set when projected on the axes. The principal components are the set of new ordered basis vectors.

To find the principal components is to compute the sample covariance matrix S of the data set and then find its eigenstructure $SU=U\Lambda$. U is a DxD matrix which has the unit length eigenvectors $u_1,\ldots,u_d$ as its columns, and Λ is a diagonal matrix with the corresponding eigenvalues $\lambda_1,\ldots,\lambda_d$. The eigenvectors are the principal components and the eigenvalues their corresponding projected variances [18].

In most applications of statistical shape analysis in the medical imaging domain, the size of the training population N is very small relative to the dimensionality of the data D. It is possible to reduce the computational load of PCA algorithm by considering the covariance matrix induced by the training set.

The covariance matrix of the data can be written as:

$$\mathbf{S} = \frac{1}{N}(\mathbf{t_n} - \boldsymbol{\mu})(\mathbf{t_n} - \boldsymbol{\mu})^t$$

Let **T** be the *N*x*N* matrix:

$$\mathbf{T} = \frac{1}{N}(\mathbf{t_n} - \boldsymbol{\mu})^t(\mathbf{t_n} - \boldsymbol{\mu})$$

Let $\mathbf{e_i}$ be the *N* eigenvectors of **T** with corresponding eigenvalues λ_i, sorted in descending order. It can be showed that the *N* vectors $(\mathbf{t_n} - \boldsymbol{\mu})\mathbf{e_i}$ are all eigenvectors of **S** with corresponding eigenvalues λ_i, and that all remaining eigenvectors of **S** have zero eigenvalues [5].

To evaluating the quality of a shape model, three measures are normally performed:

- Compactness: this measure describes how many parameters are needed to describe the instances in the training set. A good model should only need a few parameters, and thus the variance of the model should be as little as possible. This is computed by summing the eigenvalues of the shape covariance matrix.
- Generalization: This measures the ability of the model to represent unknown instances. This measure can be obtained with a leave-one-out analysis, which consists on representing a left-out instance from the set of N-1 training shapes.
- Specificity: When synthesising artificial shapes by sampling in the learned distribution, the results should be similar to the shapes found in the training set. This can be validated by generating a range of instances and comparing them to the training set.

2.3 Reconstructing Shape from Sparse Surface Point Information

Once the shape model has been constructed, the goal is to obtain from sparse surface point information the complete patient-specific 3D shape. In other words, one needs to extrapolate from sparse point information to a dense surface describing the complete 3D shape. Our model fitting algorithm is formulated as a least squares error minimization with additional regularization terms that computes the Mahalanobis distance of the predicted model [21]. The Mahalanobis distance term enables stable prediction with minimal number of known surface points. A more detailed explanation of the algorithm can be found in [21]. Here, a summary of the algorithm is presented:

- Initially a small point-set of anatomical landmarks with known correspondence to the model is digitized. This is used to register the patient anatomy to the model. This also provides an initial estimation of the 3D shape with only a few digitized points.
- To improve the prediction, additional points can be interactively incorporated via closest distance correspondence. The objective function that we minimize is defined as follows:

$$f = \rho\left\{\sum_{\substack{k=1 \\ j=Index(k)}}^{n} w_k \left\| Y_k - \left(\overline{X}_j + \sum_{i=1}^{m} \alpha_i u_i(j) \right) \right\|^2 \right\} + (1-\rho)\left\{\sum_{i=1}^{m} \frac{\alpha_i^2}{\lambda_i}\right\}$$

The first term in the function is the Euclidean distance between the *n* digitized points *Y* and the estimated shape comprising the mean shape *X* plus a weighted sum of the eigenvectors u_i. The corresponding point for each of the digitized points Y_k is computed using closest point correspondence from the current estimated shape. This is denoted as $\overline{X}_j$, where *j = Index(k)* is the index of the closest point corresponding to the *k*th digitized point. The second term is the Mahalanobis distance of the predicted shape from the mean and controls the probability of the predicted shape. This term ensures that the predicted shapes are valid by favouring those that are closer to the mean.

The parameter ρ in the objective function enables the deformation scheme to have better convergence behaviour. This is enabled by relaxing the effect of the Mahalanobis distance term as additional points are digitized. This makes the surface less constrained to remain close to the mean and allows it to more freely deform.

3. Experimental Results

3.1 Morphological Analysis of Proximal and Left Human Femurs

We present results obtained from a training set of 30 surface models extracted from CT data. These models represent complete left human femurs and proximal femurs, respectively, and are used in on-going research at our institute for computer-assisted surgery, such as total hip replacement (THR), total knee arthroplasty (TKA), and anterior cruciate ligament surgery (ACL).

Correspondences across data sets were established via a semiautomatic process in which a set of analogous anatomical landmarks (points, lines or surfaces) are identified in all data, and the remaining points are evenly spread to cover the surface of the object. These correspondences are further optimised via a Minimum Description Length (MDL)

optimisation [5]. For further processing, each object is represented by a dense 3D point cloud. Figure 1 shows the first and second modes of variation found for proximal femurs.

From Figure 1 it can be seen that the first PCA mode mainly describes the deformation of the femoral head, whereas the second mode of variation describes a global scaling of the structure. Figure 2 shows the results obtained in terms of compactness, generalization and specificity. In addition, error measurements for different methods used to find point correspondences are reported for femoral head. As mentioned in the introductory section, MDL outperformed other methods.

Statistical shape analysis of left human femurs was also performed. The training dataset consisted of 32 surface models extracted from CT data. For illustrative purposes, Figure 3 shows for one case the original CT data, the segmented femur, and the surface rendering of the segmented image. As for the case of human proximal femurs, point correspondences were computed in the same way and then a principal component analysis was carried out.

Figures 4 to 6 present the first three modes of variation. In each image, blue lines correspond to vectors indicating direction of the deformation at each point on the surface. In addition, the magnitude of the deformation was mapped in colours for better visualization.

3.2 Dry Cadaver Femur Data

Nine different dry cadaver femur bones were chosen for this validation study. High-resolution CT scans of these bones were segmented (image resolution: 0.652 x 0.652 x 1.0 mm) and fine 3D surface models were generated. The experiment trials were carried out in the CT coordinate system. The three anatomical landmarks and additional 51 bone surface points were digitized on the surface model of each of the cadaver bones. The deformation procedure was then employed to estimate the 3D model that best approximates the digitized set of points. We carried out the experiments on two models, built from different initial training populations. The first model was constructed from the entire training set of 30 proximal femurs and the second model was constructed from a subset of 14 proximal femurs, with correspondence optimized across the respective training sets. This helped us to evaluate the effect of training size on the deformation algorithm. Table 1 shows the error results for each of the cadaver bones with different number of digitized surface points using the larger and smaller population. The mean surface errors with 3, 27 and 54 selected surface points are tabulated.

Figure 7 shows the statistics cumulated for the 9 cadaver bones. The average of the mean and median errors across the entire set of 9 cadaver bones is plotted against the number of digitized points for both models generated from smaller and larger populations. The average mean surface error with 10 digitized points lies between 2.1-2.6mm and with 54 digitized points the error is 1.7-1.9mm.

Table 1. Mean surface errors for nine dry cadaver bones with 3, 27 and 54 selected surface points in the CT-based error scheme. The errors are tabulated for both experiments with larger smaller populations.

	Mean error [mm] w.r.t # of points					
Bone #	**Large population**			**Small population**		
	3	27	54	3	27	54
1	2.08	1.90	1.72	2.57	2.02	1.85
2	0.96	0.91	0.85	2.03	1.49	1.23
3	2.44	2.28	2.00	3.02	2.69	2.5
4	2.55	2.45	2.03	2.92	2.63	2.12
5	2.18	1.99	1.85	1.98	1.87	1.72
6	3.49	3.10	2.54	4.44	3.79	2.65
7	1.73	1.59	1.39	3.15	2.61	2.23
8	2.01	1.87	1.67	1.91	1.75	1.58
9	2.06	2.04	1.83	2.22	2.14	1.64
Average	2.17	2.04	1.83	2.22	2.14	1.64

4. Conclusion

Statistical shape analysis has shown to be an important tool to improve shape prediction when only sparse data is available. Furthermore, it has been shown how multivariate statistical analyses can assist at focusing on the relevant shape variation among a population, thus bringing more efficacy and accuracy to surgery planning.

We presented a model that employs point distribution models (PDM) for the representation of shapes. We solved the point correspondence starting from a shape-based surface correspondence (MSS), which we further optimized using a Minimum Description Length (MDL) criterion. For the model fitting algorithm we employed the Mahalanobis distance of the predicted model to regularize a least square error minimization. We highlighted the relevance of choosing an appropriate point-correspondence method, as well as that of a suitably-sized the training set.

We showed quantitatively and qualitatively how statistical shape models of human femurs are built and how these models are used in computer assisted surgery in order to minimize the invasiveness on patients.

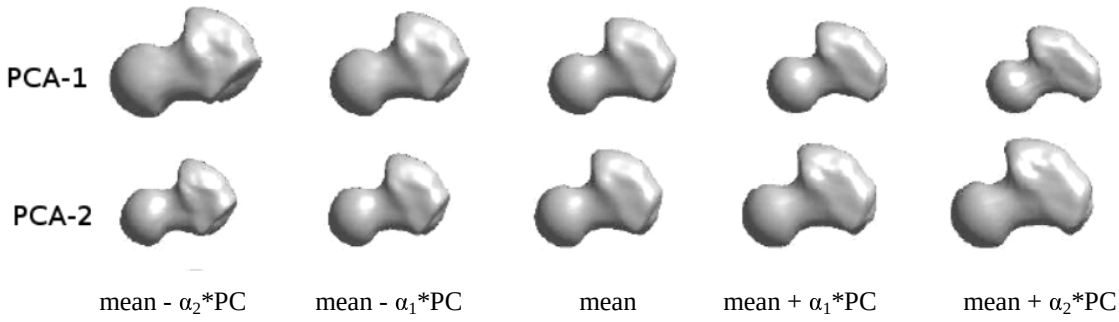

Figure 1. Shape analysis of human proximal femurs. The first two rows correspond to the first and second principal components, PCA-1 and PCA-2 respectively. The two figures to the right have a decreasing weighting on each principal component, and the figures to the left an increasing negative weight ($\alpha_2 > \alpha_1$).

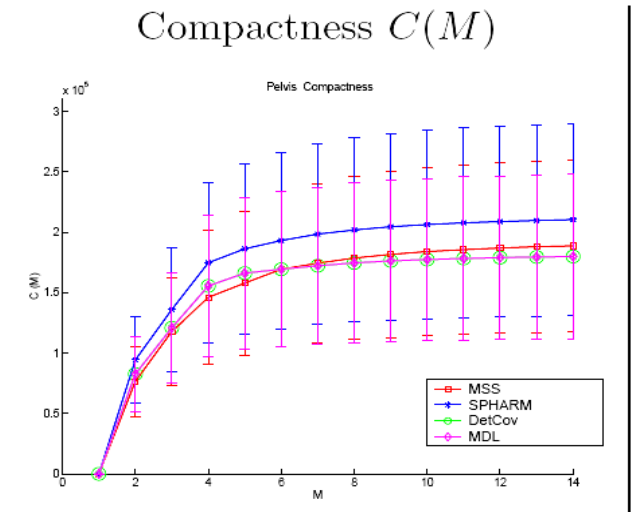

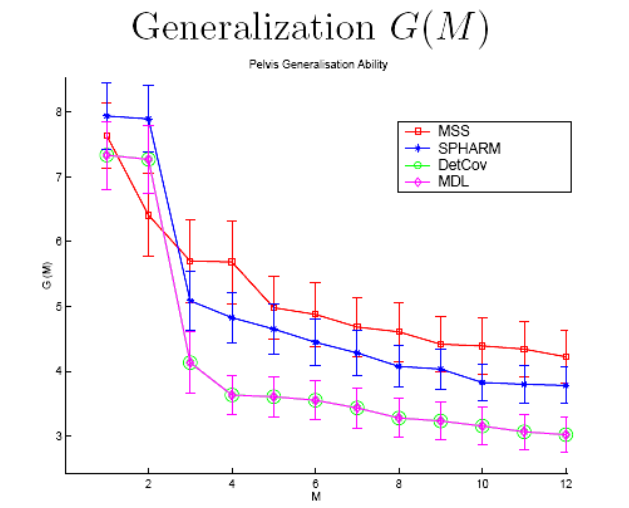

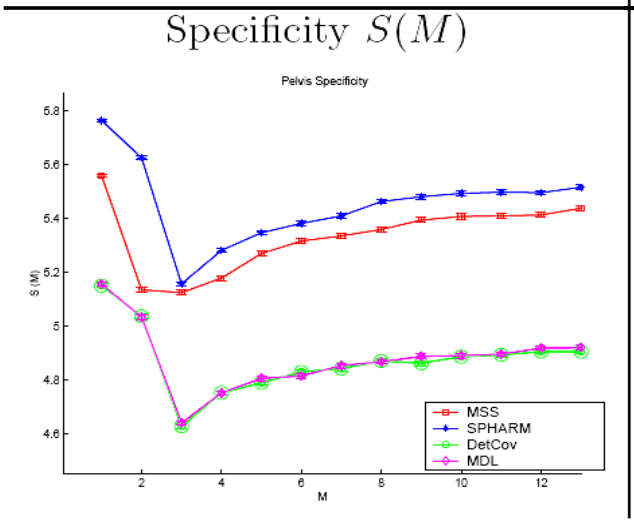

Landmark error table

Method	Femoral head		
	Mean	Max	Min
MSS	3.13 mm	6.48 mm	1.73 mm
SPHARM	7.24 mm	12.2 mm	6.07 mm
DetCov	3.24 mm	7.36 mm	1.71 mm
MDL	3.40 mm	6.41 mm	1.71 mm

Figure 2*: Top row and bottom left: Graphs with error plots of compactness (C(M)), generalization (G(M)) and specificity (S(M)) for the femoral head study. Bottom row, right: Table with average, maximal and minimal mean absolute distances (MAD) between the manual landmarks and the studied methods for the femoral head study.*

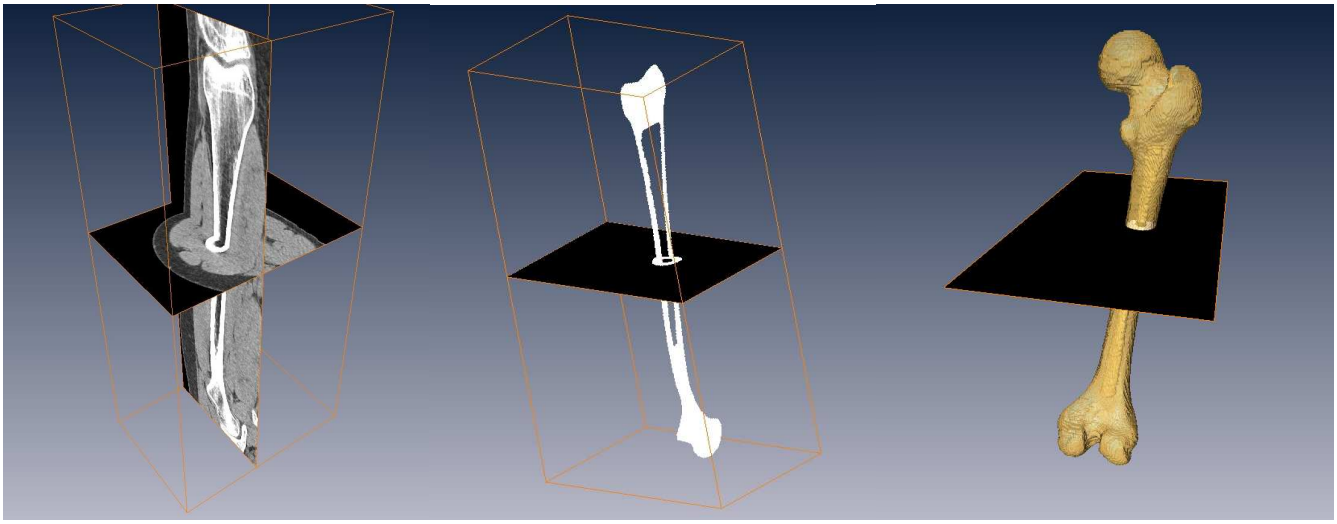

***Figure 3**. Example of input data in the training dataset used to build the statistical shape model of left human femur. Leftmost image corresponds to transversal and longitudinal planes of the original CT data. The segmented bone surface (central image) and a surface rendering of the segmentation (rightmost image) are shown for illustrative purposes.*

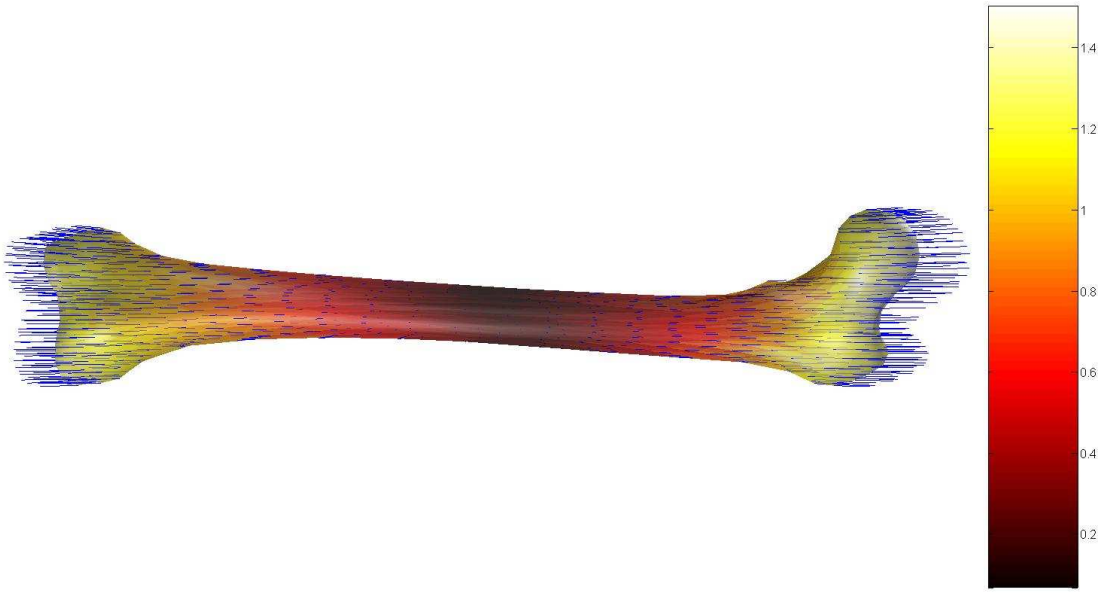

***Figure 4**: First mode of variation for left femur. Clearly the predominant mode of variation is the change in length of femurs.*

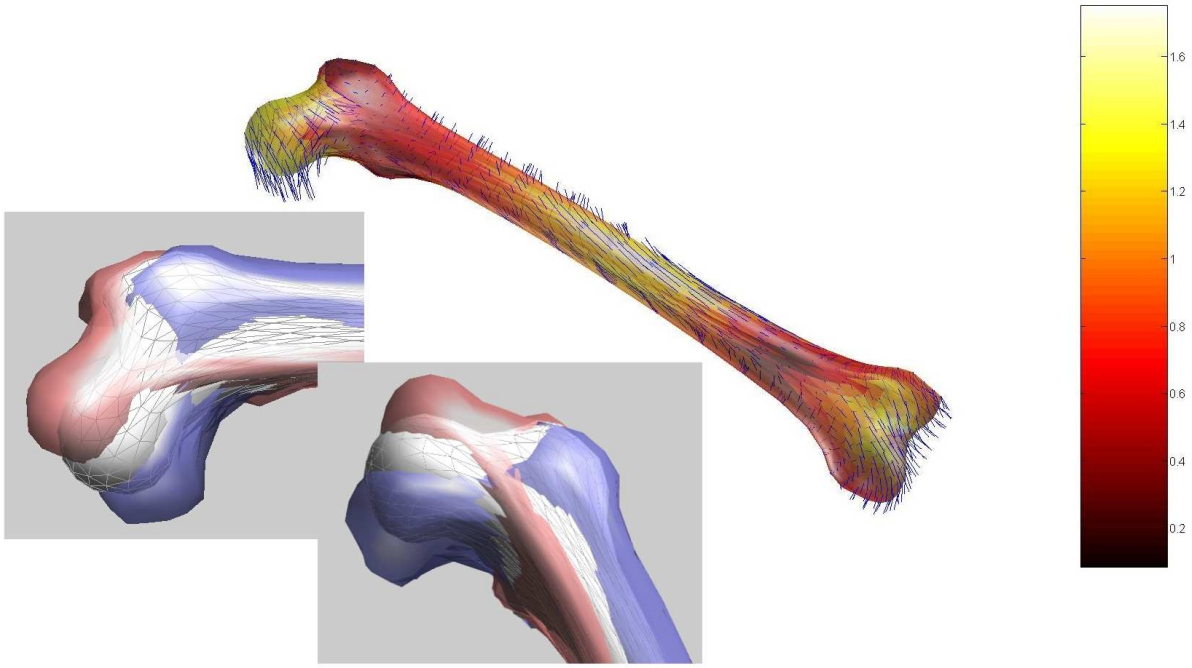

Figure 5: *Second mode of variation for left femur. Two different views of the zoomed region-of-interest (i.e., where deformations are more important) show the range of deformation in that area. It can be seen that this mode rules the inclination of the femoral head.*

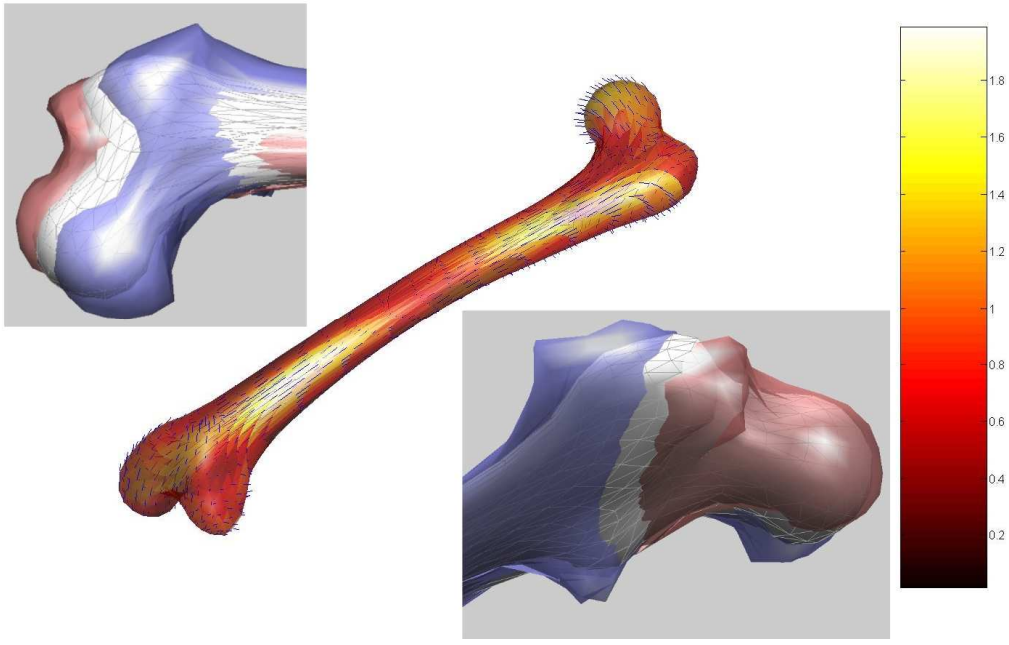

Figure 6: *Third mode of variation for left femur. Compared to the first two modes, the third mode is harder to interpret. This mode describes a deformation of the posterior part of the femoral head and a slight torsion and curvature of the central region (this is better observed in an image sequence)*

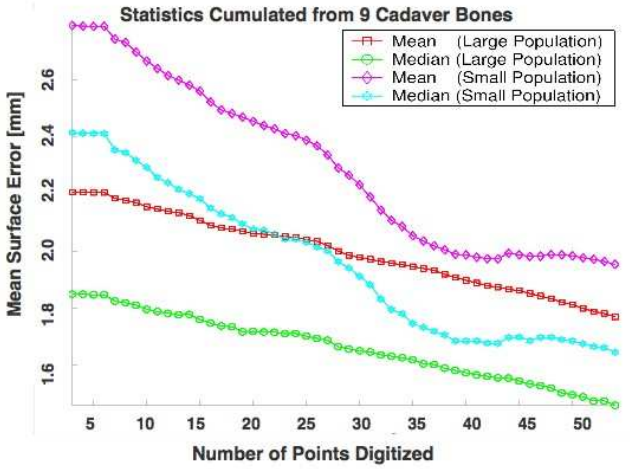

Figure 7: *Error statistics cumulated across all the cadaver bones. The average mean and median errors are plotted against the number of digitized points for both the models generated from smaller and larger population.*

References

[1] González Ballester, M. A., Zisserman, A., Brady, M.: Estimation of the Partial Volume Effect in MRI. Medical Image Analysis, 6(4):389-405, 2002

[2] Bakshi, R., Benedict, R. H., Bermel, R. A., Jacobs, L.: Regional Brain Atrophy is Associated with Physical Disability in Multiple Sclerosis: Semiquantitative MRI and Relationship to Clinical Findings. Journal of NeuroImaging, 11(2):129-136, 2001

[3] Cootes, T. F., Taylor, C. J., Cooper, D. H., Graham, J.: Active Shape Models - Their Training and Applications. Computer Vision and Image Understanding, 61(2), 1995

[4] González Ballester, M. A., Zisserman, A., Brady, M.: Measurement of Brain Structures based on Statistical and Geometrical 3D Segmentation. Procs. of MICCAI'1998, Lecture Notes in Computer Science, 1496:499-508, 1998

[5] Cootes, T. F., Edwards, G. J., Taylor, C. J.: Active Appearance Models. IEEE Transactions on Pattern Analysis and Machine Intelligence, 23(6):681-685, 2001

[6] Fleute, M., Lavallée, S. Building a complete surface model from sparse data using statistical shape models. Vol. 1496 of Lecture Notes in Computer Science, Proceedings of Medical Image Computing and Computer Assisted Interventions. pp. 879–887, 1998

[7] Stindel, E., Briard, J., Merloz, P., Plaweski, S., Dubrana, F., Lefevre, C., Troccaz, J. Bone morphing: 3D morphological data for total knee arthroplasty. Computer Aided Surgery 7 (3), 156–168, 2002

[8] Chan, C. S., Edwards, P. J., Hawkes, D. J. Integration of ultrasoundbased registration with statistical shape models for computer-assisted orthopaedic surgery. Proceedings of SPIE Medical Imaging. pp. 414–424, 2003

[9] Rajamani, K. T., Nolte, L., Styner, M. Bone morphing with statistical shape models for enhanced visualization. Proceedings of SPIE Medical Imaging. pp. 122–130, 2004

[10] Bookstein, F. L. Size and shape spaces for landmark data in two dimensions. Statistical Science 1, 181–242. 1986

[11] Kelemen, A., Székely, G., Gerig, G., October. Elastic model-based segmentation of 3D neuroradiological data sets. IEEE Transactions on Medical Imaging. 18, 828–839, 1999

[12] Heitz, G., Rohlfing, T., Maurer, C. Statistical shape model generation using nonrigid deformation of a template mesh. Vol. 5747 of Proceedings of SPIE Medical Imaging. pp. 1411–1421. 2005

[13] Brechbühler, C., Gerig, G., K¨ubler, O. Parametrization of closed surfaces for 3-D shape description. Computer Vision and Image Understanding 61 (2), 154–170. 1995

[14] Kotcheff, A., Taylor, C. Automatic construction of eigenshape models by direct optimization. Vol. 2 of Medical Image Analysis. pp. 303–314. 1998

[15] Davies, R. H., Twining, C. J., Cootes, T. F., Waterton, J. C., Taylor, C. J. A minimum description length approach to statistical shape modeling. IEEE Transaction on Medical Imaging 21 (5), 525–537. 2002

[16] Wang, Y., S., P. B., Staib, L. H. Shape-based 3D surface correspondence using geodesics and local geometry. Proceedings of Computer Vision and Pattern Recognition. pp. 644–651. 2000

[17] Styner, M. A., Rajamani, K. T., Nolte, L. P., Zsemlye, G., Szekely, G., Taylor, C. J., Davies, R. H. Evaluation of 3D correspondence methods for model building. Proceedings of Information Processing in Medical Imaging. pp. 63–75. 2003

[18] Svensén, J. F. M.: GTM: The Generative Topographic Mapping. PhD Thesis, Aston University, 1998

[19] Fodor, I.K.: A Survey of Dimension Reduction Techniques. Lawrence Livermore National Laboratory Technical Report no. UCRL-ID-148494, 2002

[20] Cootes, T. F., Edwards, G. J., Taylor, C. J.: Active Appearance Models. IEEE Transactions on Pattern Analysis and Machine Intelligence, 23(6):681-685, 2001

[21] Rajamani, K., González Ballester, M., Nolte, L., Styner, M. A novel and stable approach to anatomical structure morphing for intraoperative 3D visualization. Vol. 5744 of Proceedings of SPIE Medical Imaging. pp. 718–725. 2005.